Dynamic Response Of Two Interacting Extensible Barsin Frictional Contact

Molenkamp, T.; Tsetas, A.; Tsouvalas, A.; Metrikine, A.

DOI
10.47964/1120.9020.19224

Publication date
2020

Document Version
Final published version

Published in
EURODYN 2020 XI International Conference on Structural Dynamics

Available online at www.easdprocedia.org
EASD Procedia EURODYN (2020) 252-264

EASD Procedia

EURODYN 2020
XI International Conference on Structural Dynamics
M. Papadrakakis, M. Fragiadakis, C. Papadimitriou (eds.)
Athens, Greece, 23–26 November 2020

DYNAMIC RESPONSE OF TWO INTERACTING EXTENSIBLE BARS IN FRICTIONAL CONTACT

Timo Molenkamp[1], Athanasios Tsetas[1], Apostolos Tsouvalas[1] and Andrei V. Metrikine[1]

[1] TU Delft
Faculty of Civil Engineering
Stevinweg 1, 2628 CN Delft
T.Molenkamp@tudelft.nl

Keywords: Pile Dynamics, Normal modes, Regularized Coulomb friction

Abstract. *In this paper, a new model is developed to describe the nonlinear dynamics of two axially deformable bars sliding relative to each other in which the interaction is governed by friction. The first bar is fixed at one end and is subjected to a distributed normal force perpendicular to its axis to activate friction at the common interface, while the second bar is allowed to slide relative to the fixed one. A semi-analytical solution method is developed in which only the nonlinear interaction is addressed numerically. The dynamic behaviour of the bars is expressed as a summation of vibration modes including the necessary rigid body mode to allow for the permanent sliding of one bar relative to the other. This results in a computationally efficient scheme without compromising the accuracy of the solutions. The developed model can be used in pile driveability studies. In this case the fixed bar resembles the soil column while the second bar describes the dynamics of the driven pile.*

ISSN:2311-9020
Peer-review under responsibility of the Organizing Committee of EURODYN 2020.
doi: 10.47964/1120.9020.19224

1 INTRODUCTION

In many engineering fields, including the field of pile driving, friction plays an important role. For example, accurate prediction of underwater noise generated in the seawater during the process of pile driving with vibratory devices requires the simultaneous prediction of the pile progression into the soil and, thus, the incorporation of a proper frictional model to describe the pile-soil slip behaviour. State of the art models in underwater noise prediction for impact pile driving all assume perfect contact between pile and soil [1, 2]. Problems including high frequency bands solved with a fixed FE-mesh, need both a fine spatial and time discretization to describe the propagating waves. This results in enormous computational efforts upto insolvable problems [2]. As a first step towards the development of a computational efficient model that predicts noise during vibratory pile driving including slippage of the pile, the dynamics of two elastic bars in frictional contact is studied in this paper.

The inclusion of friction complicates the problem, as it introduces a strong nonlinearity. To describe the forces at a frictional interface an appropriate frictional law should be chosen [3]. Since the focus herein is on noise generated during the driving process of piles with vibratory devices, the interest is in a straightforward frictional model that can describe the sliding between pile and soil. The most common frictional model is based on the Coulomb friction law. Coulomb's friction can be applied in many fields such as in a simplified model for belt driving mechanics, in which the Coulomb's friction law represents the dry friction between belt and support [4]. Variations on Coulomb's friction for multi-body mechanicals systems are described for example by Marques et al. [5]. The Coulomb friction, which is multivalued at zero velocity, can be approximated by alternative methods which deviate from Coulomb's friction below a certain velocity threshold and have a finite slope at zero velocity, e.g. linear velocity-dependent friction at low velocities and an approximation by a hyperbolic tangent [5]. Another alternative is introduced by Threlfall, the method avoids the discontinuity in the transition between positive and negative and it has a higher resemblance with the Coulomb friction law at velocities below a certain threshold [6]. This last friction law fits the problem of vibratory pile driving since it is smooth and the pile is assumed to slide continuously to the soil, while sticking can be neglected.

The model discussed in this work can be seen as a predecessor of a three-dimensional model to be used in pile driving noise prediction including the effect of pile-soil slip. In section 2, the problem statement is explained, including the equations of motions, boundary conditions and Threlfall's friction law. Hereafter, the solution method is described. The solution approach is largely analytical; a numerical scheme is used only to evaluate standard integrals. Section 3 describes the limitations of the method in terms of convergence, including criteria for the truncation of the number of modes that are used in this work. Section 4 shows results for the case of an impact load represented by a block function and a harmonic load. Finally, section 5 contains conclusions regarding the model performance.

2 MATHEMATICAL FORMULATION

2.1 Governing equations

The model under consideration is schematized in Fig. 1. It consists of two bars, which can deform in the axial direction and interact through a frictional interface. The equations of motion

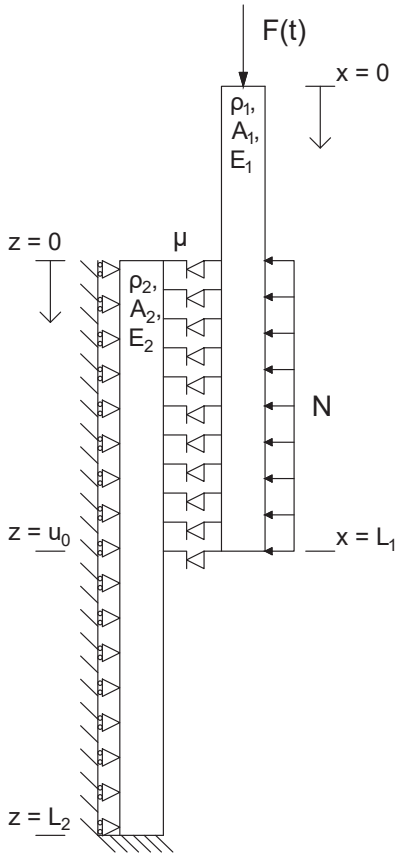

Figure 1: Schematization of the problem statement

describing the dynamics of the two bars read:

$$\rho_1 A_1 \ddot{u}_1(x,t) = E_1 A_1 u_1''(x,t) - T_1(x,t) + F(t)\delta(x) \tag{1}$$

$$\rho_2 A_2 \ddot{u}_2(z,t) = E_2 A_2 u_2''(z,t) - T_2(z,t) \tag{2}$$

in which subscript 1 refers to the forced bar and subscript 2 to the constrained bar, hereafter called bar 1 and 2. The constants ρ, A and E define the density, area and elasticity of the bars respectively. $T_{1,2}(x,t)$ represents the friction that acts on either bar. The driving force $F(t)$ can alternatively be included in a time-dependent boundary [7], however, the interest here lies not in the precise description of the top boundary stresses. A local coordinate system is adopted for bar 1. The progression of the lower end of bar 1 with respect to the upper end of bar 2 is characterized by $u_0(t)$ as shown in Fig. 1. The prime and dot indicate derivatives with respect to spatial coordinates and time, respectively. Threlfall's friction law is adopted, i.e. the signum function that is smoothed around zero velocity:

$$T_1(x,t) = \mu N \operatorname{sgn}(\Delta v_1(x,t)) \left(1 - e^{-k\frac{\Delta v_1(x,t)}{v_{95}}}\right) H(x - L_1 + u_0(t)) \tag{3}$$

$$T_2(z,t) = \mu N \operatorname{sgn}(-\Delta v_2(z,t)) \left(1 - e^{-k\frac{\Delta v_2(z,t)}{v_{95}}}\right) H(u_0(t) - z) \tag{4}$$

with:

$$\Delta v_1(x,t) = \dot{u}_1(x,t) - \dot{u}_2(x - L_1 + u_0(t), t) \tag{5}$$

$$\Delta v_2(z,t) = \dot{u}_2(z,t) - \dot{u}_1(z + L_1 - u_0(t), t) \tag{6}$$

where H is the Heaviside function and v_{95} is a velocity threshold above which the friction behaves almost velocity independent, i.e. at $\Delta v = v_{95}$: $T \approx 0.95 T_{max}$ for $k = 3$. The velocity threshold is based on the maximum modal change of velocity amplitude per time step, derived based on the results of section 2.2 of this paper as:

$$v_{95} = \frac{4\mu N \Delta t}{\pi \rho_1 A_1} \tag{7}$$

The boundary conditions read:

$$u_1'(0,t) = u_1'(L_1,t) = u_2'(0,t) = u_2(L_2,t) = 0 \tag{8}$$

The initial conditions are:

$$u_1(x,t_0) = u_{t_0}, \quad \dot{u}_1(x,t_0) = \dot{u}_{t_0}, \quad u_2(x,t_0) = w_{t_0}, \quad \dot{u}_2(x,t_0) = \dot{w}_{t_0} \tag{9}$$

Eqs. (1) to (9) govern the dynamics of the coupled system in the time domain.

2.2 Solution method

A modal solution approach is adopted, therefore, the displacements are expressed as a summation of modes:

$$u_1(x,t) = \sum_{n=1}^{\infty} \phi_n(x)\eta_n(t), \qquad u_2(z,t) = \sum_{m=1}^{\infty} \psi_m(z)\zeta_m(t) \tag{10}$$

Bar 1 is allowed to slide with respect to bar 2; the relative motion is governed by the rigid body motion of bar 1; relative displacement due to deformation of either bar is neglected. Substitution of Eq. (10) into Eqs. (1) and (2) yields:

$$\sum_{n=1}^{\infty} \phi_n(x)\ddot{\eta}_n(t) + \omega_n^2 \phi_n(x)\eta_n(t) = \frac{F(t)\delta(x) - T_1(x,t)}{\rho_1 A_1} \tag{11}$$

$$\sum_{m=1}^{\infty} \psi_m(z)\ddot{\xi}_m(t) + \omega_m^2 \psi_m(z)\xi_m(t) = -\frac{T_2(z,t)}{\rho_2 A_2} \tag{12}$$

with:

$$\phi_n(x) = \cos\left(\frac{\omega_n x}{c_1}\right), \qquad \omega_n = \frac{n\pi c_1}{L_1} \qquad n = 0,1,2,... \tag{13}$$

$$\xi_m(z) = \cos\left(\frac{\omega_m z}{c_2}\right), \qquad \omega_m = \frac{(2m-1)\pi c_2}{2L_2} \qquad m = 1,2,3,... \tag{14}$$

being the spatial eigenfunctions satisfying Eqs. (8). Eqs. (11) and (12) are multiplied by another mode and integrated over the length of each bar, making use of the orthogonality relation of the modes. After substituting Eqs. (3) and (4) into Eqs. (11) and (12), one obtains:

$$\ddot{\eta}_n(t) + \omega_n^2 \eta_n(t) = \frac{1}{\rho_1 A_1 a_n}\left(F(t) - \mu N \int_{L_1 - u_0(t)}^{L_1} \phi_n(x)\,\mathrm{sgn}(\Delta v_1(x,t)) \times \left(1 - e^{-k\frac{\Delta v_1(x,t)}{v_{95}}}\right)\mathrm{d}x\right) \tag{15}$$

$$\ddot{\xi}_m(t) + \omega_m^2 \xi_m(t) = -\frac{\mu N}{\rho_1 A_1 a_m}\int_0^{u_0(t)} \psi_m(z)\,\mathrm{sgn}(\Delta v_2(z,t))\left(1 - e^{-k\frac{\Delta v_2(z,t)}{v_{95}}}\right)\mathrm{d}z \tag{16}$$

with:

$$a_n = \int_0^{L_1} \phi_n(x)^2 \mathrm{d}x = \begin{cases} L_1 & n = 0 \\ \frac{1}{2} L_1 & n \neq 0 \end{cases}, \quad a_m = \int_0^{L_2} \psi_m(z)^2 \mathrm{d}z = \frac{1}{2} L_2 \tag{17}$$

To facilitate a computationally efficient solution of Eqs. (15) and (16), a straightforward time-stepping scheme is chosen, assuming that the relative velocity, $\Delta v_{1,2}(z,t)$, and the progression $u_0(t)$ are constant during a time step. Under the stated assumptions, Eqs. (15) and (16) act linear during a time step and the modal amplitudes η_n and ξ_m can be found using the Duhamel's integral for each time step. The closed-form solution to Eq. (15) reads:

$$\begin{aligned} \eta_n(t_{i+1}) = {} & A_n \sin(\omega_n t_{i+1}) + B_n \cos(\omega_n t_{i+1}) \\ & + \frac{1}{\omega_n a_n \rho_1 A_1} \int_{t_i}^{t_{i+1}} F(\tau) \sin(\omega_n (t_{i+1} - \tau)) \mathrm{d}\tau - \frac{\mu N \left(1 - \cos(\omega_n \Delta t)\right)}{\omega_n^2 a_n \rho_1 A_1} \\ & \times \int_{L_1 - u_0(t_i)}^{L_1} \phi_n(x) \operatorname{sgn}(\Delta v_1(x, t_i)) \left(1 - e^{-k \frac{\Delta v_1(x,t_i)}{v_{95}}}\right) \mathrm{d}x \end{aligned} \tag{18}$$

in which A_n and B_n are found by the previous time step:

$$\begin{aligned} A_n &= \frac{\sin\left(\omega_n t_i\right) \omega_n \eta_n(t_i) + \cos\left(\omega_n t_i\right) \dot{\eta}_n(t_i)}{\omega_n} \\ B_n &= \frac{\cos\left(\omega_n t_i\right) \omega_n \eta_n(t_i) - \sin\left(\omega_n t_i\right) \dot{\eta}_n(t_i)}{\omega_n} \end{aligned} \tag{19}$$

and in the special case of the initial time step:

$$\eta_n(t_0) = \frac{\int_0^{L_1} u_{t_0} dx}{a_n}, \qquad \dot{\eta}_n(t_0) = \frac{\int_0^{L_1} \dot{u}_{t_0} dx}{a_n} \tag{20}$$

The time derivative of $\eta_n(t)$ is given as:

$$\begin{aligned} \dot{\eta}_n(t_{i+1}) = {} & A_n(t_i) \omega_n \cos(\omega_n t_{i+1}) - B_n(t_i) \omega_n \sin(\omega_n t_{i+1}) \\ & + \frac{1}{a_n \rho_1 A_1} \int_{t_i}^{t_{i+1}} F(\tau) \cos(\omega_n (t_{i+1} - \tau)) \mathrm{d}\tau - \frac{\mu N \sin(\omega_n \Delta t)}{\omega_n a_n \rho_1 A_1} \\ & \times \int_{L_1 - u_0(t_i)}^{L_1} \phi_n(x) \operatorname{sgn}(\Delta v_1(x, t_i)) \left(1 - e^{-k \frac{\Delta v_1(x,t_i)}{v_{95}}}\right) \mathrm{d}x \end{aligned} \tag{21}$$

with $\Delta t = t_{i+1} - t_i$. Similar procedure for ξ_m results in:

$$\begin{aligned} \xi_m(t_{i+1}) = {} & C_m(t_i) \sin(\omega_m t_{i+1}) + D_m(t_i) \cos(\omega_m t_{i+1}) \\ & - \frac{\mu N \left(1 - \cos(\omega_m \Delta t)\right)}{\omega_m^2 a_m \rho_2 A_2} \int_0^{u_0(t_0)} \psi_m(z) \operatorname{sgn}(\Delta v_2(z, t_i)) \left(1 - e^{-k \frac{\Delta v_2(z,t_i)}{v_{95}}}\right) \mathrm{d}z \end{aligned} \tag{22}$$

$$\begin{aligned} \dot{\xi}_m(t_{i+1}) = {} & C_m(t_i) \omega_m \cos(\omega_m t_{i+1}) - D_m(t_i) \omega_m \sin(\omega_m t_{i+1}) \\ & - \frac{\mu N \sin(\omega_m \Delta t)}{\omega_m a_m \rho_2 A_2} \int_0^{u_0(t_i)} \psi_m(z) \operatorname{sgn}(\Delta v_2(z, t_i)) \left(1 - e^{-k \frac{\Delta v_2(z,t_i)}{v_{95}}}\right) \mathrm{d}z \end{aligned} \tag{23}$$

Where C_m and D_m are found similar to A_n and B_n. As mentioned earlier, the spatial integrals including the friction terms need numerical evaluation. The time step needs to be chosen such that it is smaller than a tenth of the smallest period in the system: $\Delta t < 2\pi / \max(\omega_i)/10$.

2.3 Linear equivalent model

The model is compared to a fully linear model that is valid for the case of no sliding. The

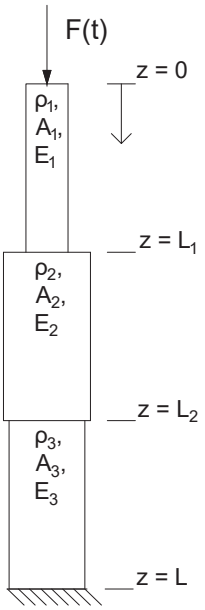

Figure 2: Schematization of the linear equivalent model

linear equivalent problem is composed of three bars as shown in Fig. 2, where the material properties of the second bar are based on the weighted averages of bar 1 and 3. The equation of motion of the whole system for each bar reads:

$$\begin{aligned} \rho_1 A_1 \ddot{u}_1 - E_1 A_1 u_1''(z,t) &= F(t)\delta(z) \qquad 0 < z < L_1 \\ \rho_2 A_2 \ddot{u}_2 - E_2 A_2 u_2''(z,t) &= 0 \qquad\qquad L_1 < z < L_2 \\ \rho_3 A_3 \ddot{u}_3 - E_3 A_3 u_3''(z,t) &= 0 \qquad\qquad L_2 < z < L \end{aligned} \tag{24}$$

The top boundary is stress-free since the applied force is accounted for in the equation of motion and the bottom boundary is fixed, furthermore, the interface conditions describe the continuity of displacements and stresses. The modes of the system can be found by solving the eigenvalue problem that is formed after substituting the general solution for each of the bars in the boundary and interface conditions. The modes are orthogonal with respect to the density and area [8]:

$$\int_0^{L_1} \rho_1 A_1 \phi_m(z)\phi_n(z)dz + \int_{L_1}^{L_2} \rho_2 A_2 \phi_m(z)\phi_n(z)dz + \int_{L_2}^{L} \rho_3 A_3 \phi_m(z)\phi_n(z)dz = a_n \delta_{nm} \tag{25}$$

The modal amplitudes are found analytically by making use of the orthogonality of the modes:

$$\eta_n(t) = A_n \sin(\omega_n t) + B_n \cos(\omega_n t) + \frac{1}{\omega_n a_n} \int_0^t F(\tau) \sin(\omega_n (t-\tau)) \mathrm{d}\tau \tag{26}$$

A_n and B_n are found by the initial conditions at $t = 0$:

$$A_n = \frac{1}{a_n \omega_n} \sum_{i=1}^{3} \int_{L_i} \rho_i A_i \phi_n(z) \dot{u}_i(z,0) dz \tag{27}$$

$$B_n = \frac{1}{a_n} \sum_{i=1}^{3} \int_{L_i} \rho_i A_i \phi_n(z) u_i(z,0) \mathrm{d}z \tag{28}$$

3 RESULTS

Two cases will be examined; the case of a block function load and the case of a high-frequency harmonic excitation. The two load cases are visualized in both time and frequency domain in Fig. 3. The material properties are chosen such that the wave speeds in both bars are

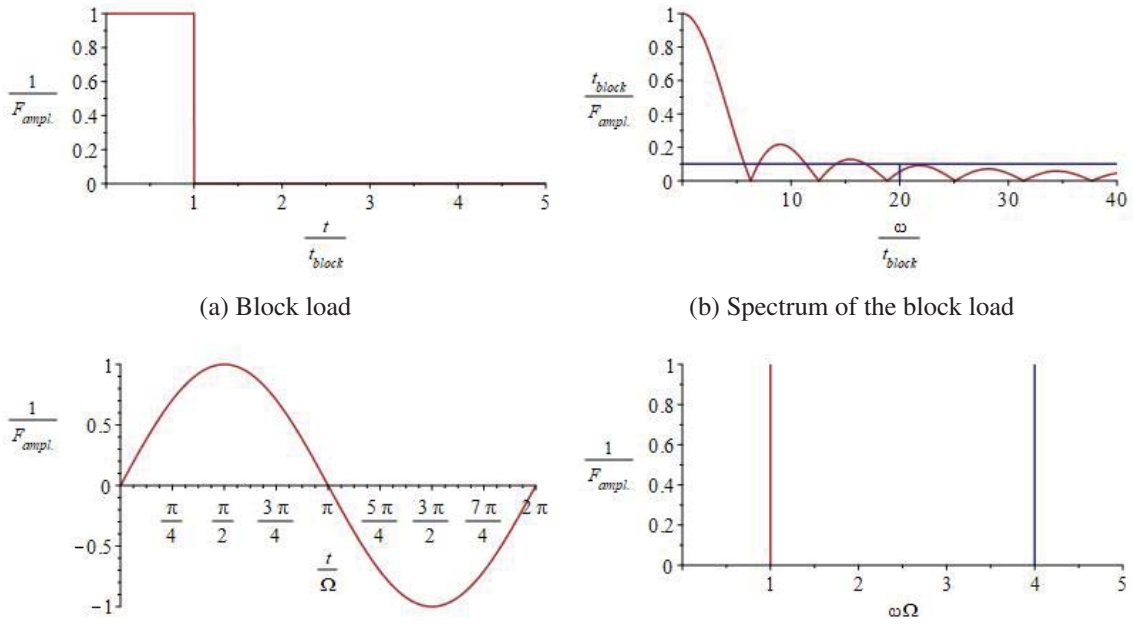

(a) Block load

(b) Spectrum of the block load

(c) Harmonic load

(d) Spectrum of the harmonic load

Figure 3: Load in time and frequency domain (red), and the minimum of frequencies included in the results (blue)

representative for steel and sandy soil. For bar 1 the properties are: $\rho_1 A_1 = 1$, $E_1 A_1 = 5000^2$, $c_1 = 5000$ and $L_1 = 20$, for bar 2: $\rho_2 A_2 = 5$, $E_2 A_2 = 500^2$ $c_2 = 500$ and $L_2 = 20$. In the initial state, the friction interface is half of bar 1, i.e. $u_0(0) = 10$. The duration of the applied block load is $t_{block} = 0.001$. The harmonic load starts at $t = 0$ with $\Omega = 1000$. The amplitude of both loads is 10. The influence of the friction coefficient μN is shown in the graphs, where μN varies from 0.1 to $100 \mu N$. $\mu N = 100$ is chosen sufficient high to approximate the linear case, where both bars move together and no sliding occurs. This case serves as validation of the description of the model with friction. The number of modes that are considered is based on the eigenfrequencies of the modes. At least frequencies excited by the block load, with an amplitude higher than 10% of the maximum amplitude or frequencies up to four times the excitation frequency of the harmonic load are included, as indicated with the blue lines in Figures 3b and 3d. For the block load and harmonic load this result in $\omega_{max} = 20.000$ and $\omega_{max} = 4.000$ respectively. This relates to about 25 and 5 flexible modes of bar 1 and about 250 and 50 modes

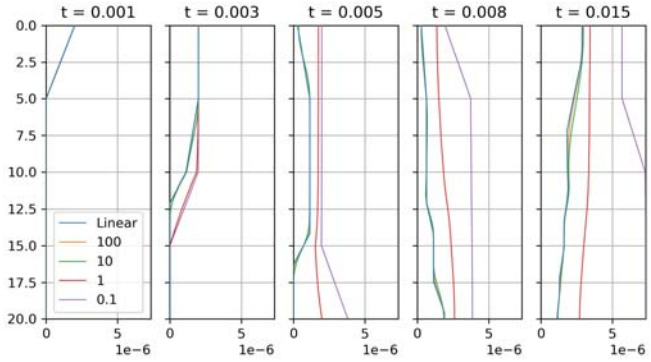

(a) Displacement of bar 1

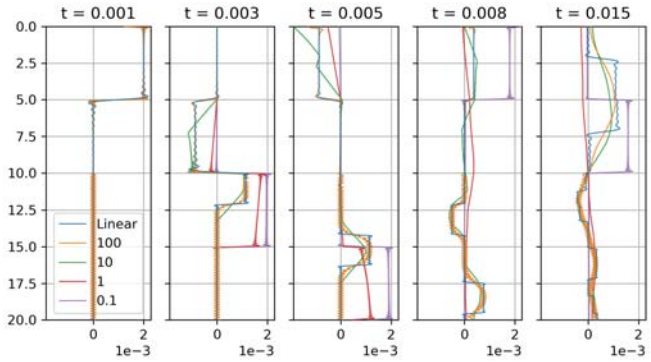

(b) Velocity of bar 1

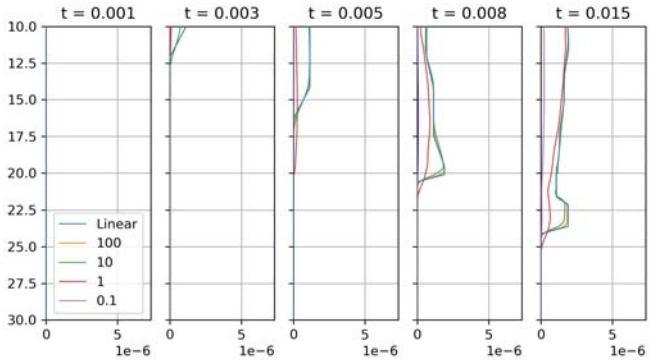

(c) Displacement of bar 2

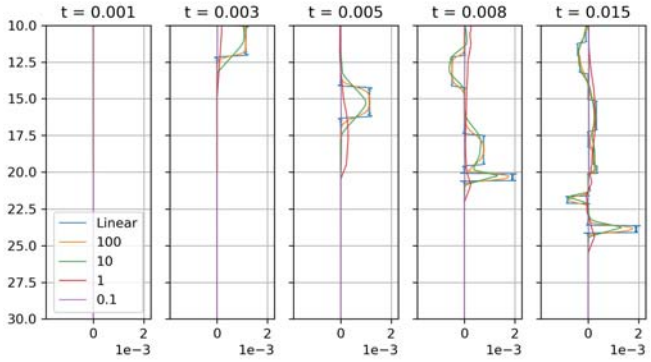

(d) Velocity of bar 2

Figure 4: The dynamic response of the bars when bar 1 is subjected to the block load for different values of μN

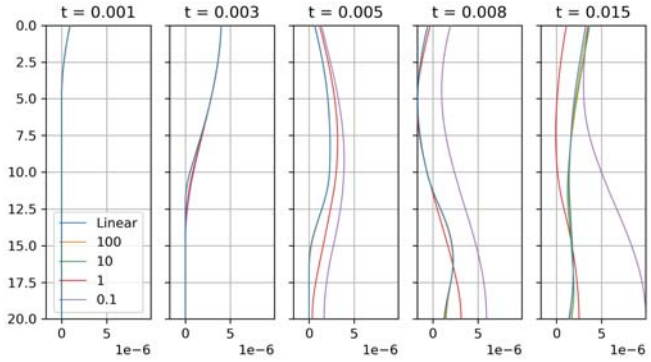

(a) Displacement of bar 1

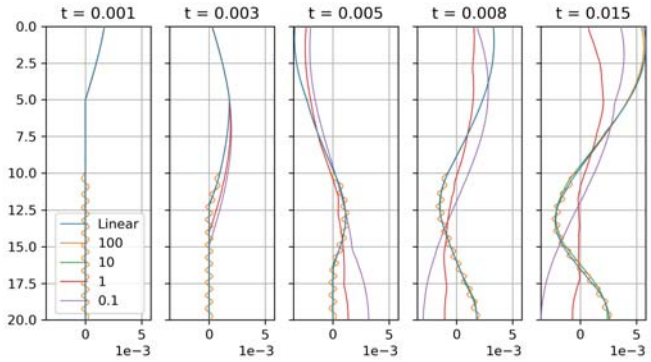

(b) Velocity of bar 1

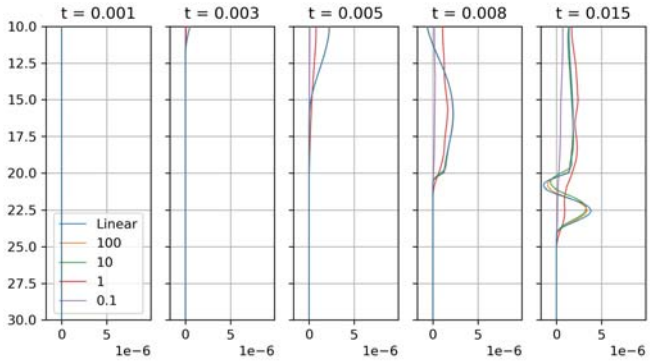

(c) Displacement of bar 2

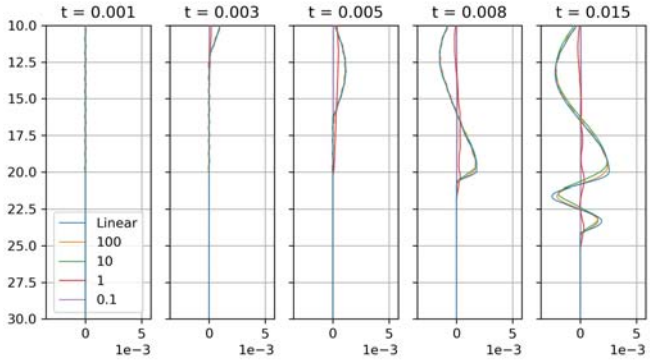

(d) Velocity of bar 2

Figure 5: The dynamic response of the bars when bar 1 is subjected to a sinusoidal load for different values of μN

for bar 2. While the friction force is based on the relative velocity of the bars, the velocities are preferably described with the same accuracy, i.e. the smallest wavelength of both bars is of the same order. Since both bars have the same length, the same number of modes are included in both bars, governed by the highest number required.

Fig. 4 shows the displacement and velocity of both bars due to a block load, representing impact pile driving. It can be seen that the block function is well represented by the summation of modes. Therefore also higher modes are activated along the whole bar. This can be seen in the amplification of higher modes, ahead of the wave-front in Fig. 4a, especially in case of high friction forces. Although present, over time these vibrations cancel out and they do not excite the system. For low friction coefficients, almost no energy dissipates into bar 1. Therefore, the wave reflects back and forth almost undisturbed.

In case of the response to a harmonic load, shown in Fig. 5, higher frequencies are not excited from the beginning, therefore, the results are more smooth. In all cases, the highest friction $\mu N = 100$ is in good agreement with the linear results. Both bars converge to the same displacement and velocity for $\mu N = 100$. Contrary, for low friction amplitudes, the unconstrained bar slides over the constrained bar. Due to that, final displacements are bigger at $t = 0.015$, best shown in Fig. 4a. Generally, the model behaves as expected, e.g. the wave-fronts align for all waves in the first bar upon the moment it starts interacting with the second bar, then for high friction amplitudes, the wave speed of both bars is based on a weighted average, whereas for low-frequency amplitudes, the wave-speed is less affected by the second bar. This is best shown in Figures 4c and 4d, where at $t = 0.004$, the three different wave-fronts are visible.

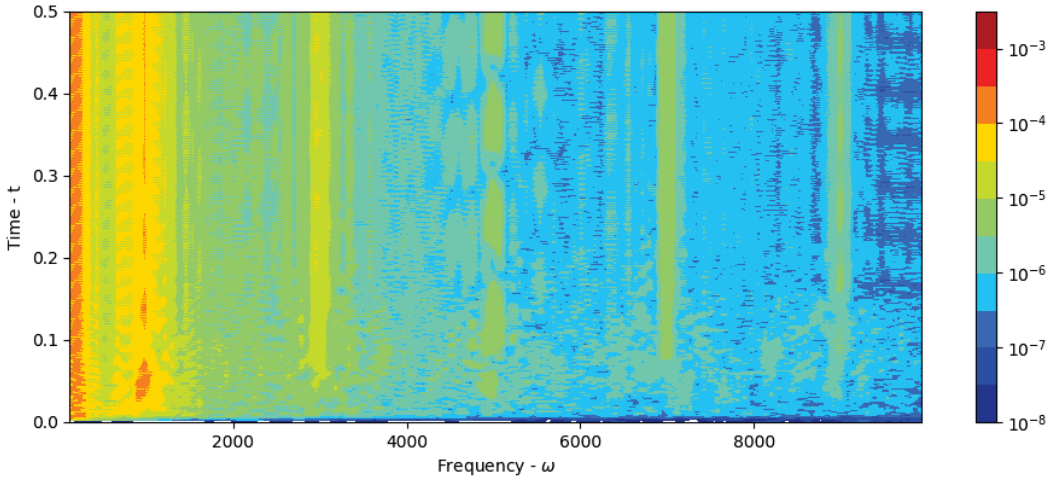

Figure 6: Time-frequency response of bar 2 for μN = 1

Fig. 6 points the importance of including the frictional interface in noise generating models for vibratory pile driving. The time-frequency plot clearly identifies the presence of the odd higher order harmonics that are excited in the system due to the presence of the frictional surface.

4 CONVERGENCE

The convergence of the model is satisfied based on displacements and velocities. The model is not able to describe the stress at the top boundary correctly due to the delta function, but the exact boundary stress at the top is not of interest, with an increasing number of modes, a

good approximation of the stress close to the boundary can be obtained. Since the time step is chosen sufficiently small: $\Delta t < 2\pi/\max(\omega_i)/10$, and depends on the number of modes in the system, the convergence of the solution depends on the truncation of the modes. The truncation criterion is based on the displacement of the bar at the final time step:

$$\delta(x, t_{i_{max}}) = \frac{\left|\sum_{n=1}^{0.9N} u_n(x,t) - \sum_{m=1}^{N} u_m(x,t)\right|}{\left|\sum_{m=1}^{N} u_m(x,t)\right|} < 1\% \tag{29}$$

where N is the number of modes. It needs to be mentioned that the convergence criterion only holds at each point from the time moment onwards when the first wave reaches the point, while before that, the denominator is zero. The convergence over time for the block load case from section 3 and $\mu N = 10$ is studied for both bars. Since the final wavefront just passed half of bar 2, only the upper half of bar 2 is taken into account. The convergence is checked between $N = 225$ and $N = 250$ modes. Fig. 7 shows that the displacements converge directly after the

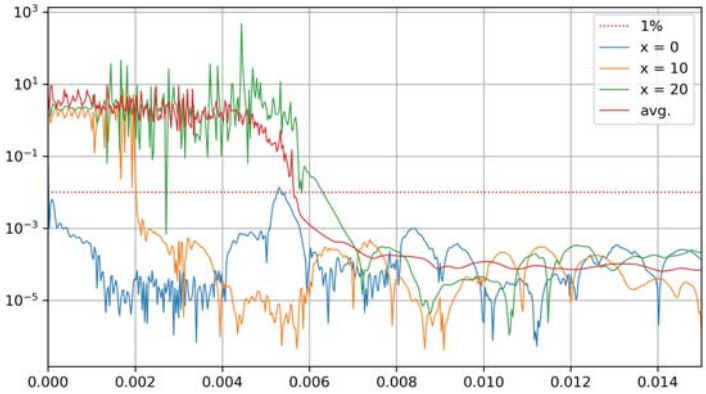

(a) $\delta(x, t_i)$ of bar 1

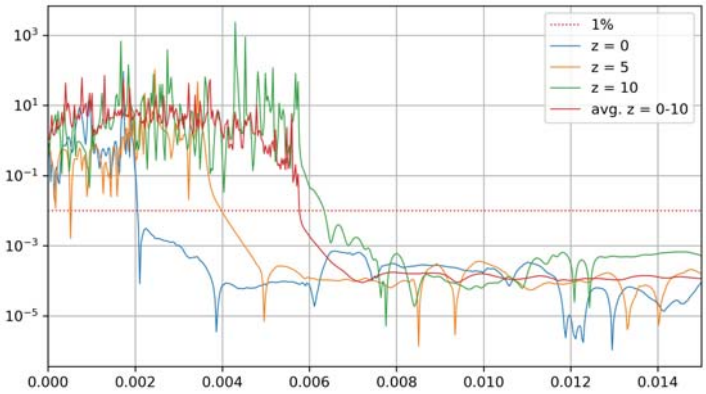

(b) $\delta(z, t_i)$ of bar 2

Figure 7: Relative error between 225 and 250 modes for $t = 0 \rightarrow 0.015$

first wavefront arrives to $\delta < 0.1\%$. It confirms that the number of modes chosen in section 3 is more than sufficient for the convergence of the displacements.

5 CONCLUSIONS

The modelling technique presented in this paper is suitable for describing the interaction of two flexible bars in frictional contact. Although stick is not included in the model, high friction forces approximate the linear model that corresponds to bars under stick condition. The accuracy of the solution increases with the number of modes included. The number of modes included is a trade-off between computational efficiency and accuracy, whereas the length of the time signal is linearly related to the computation time. More modes need to be included to approximate sudden jumps in stress or velocity. This is of major importance in impact excitations but since the work focuses on harmonic excitations, sudden jumps are not expected. Conclusively, the modelling approach seems suitable for the field of application since the excitation is mainly harmonic, the non-linear behaviour of the interface can be included without compromising the computational time compared to linear models.

6 ACKNOWLEDGEMENT

This research is associated with the GDP project in the framework of the GROW joint research program. Funding from "Topsector Energiesubsidie van het Ministerie van Econsomische Zaken" under grant number TEHE117100 and financial/technical support from the following partners is gratefully acknowledged: Royal Boskalis Westminster N.V., CAPE Holland B.V., Deltares, Delft Offshore Turbine B.V., Delft University of Technology, ECN, Eneco Wind B.V., IHC IQIP B.V., SHL Offshore Contractors B.V., Shell Global Solutions International B.V., Sif Netherlands B.V., TNO, and Van Oord Offshore Wind Projects B.V.

REFERENCE

[1] A. Tsouvalas and A. V. Metrikine. A three-dimensional vibroacoustic model for the prediction of underwater noise from offshore pile driving. *Journal of Sound and Vibrationn*, 333 (8):2283–2311, 2014. ISSN 21954364. doi: 10.1007/978-3-642-40371-2_38.

[2] Moritz B. Fricke and Raimund Rolfes. Towards a complete physically based forecast model for underwater noise related to impact pile driving. *The Journal of the Acoustical Society of America*, 137(3):1564–1575, 2015. ISSN 0001-4966. doi: 10.1121/1.4908241.

[3] E. J. Berger. Friction modeling for dynamic system simulation. *Applied Mechanics Reviews*, 55(6):535–577, 2002. ISSN 00036900. doi: 10.1115/1.1501080.

[4] M. J. Leamy, J. R. Barber, and N. C. Perkins. Distortion of a harmonic elastic wave reflected from a dry friction support. *Journal of Applied Mechanics, Transactions ASME*, 65(4):851–857, 1998. ISSN 15289036. doi: 10.1115/1.2791921.

[5] Filipe Marques, Paulo Flores, J. C. Pimenta Claro, and Hamid M. Lankarani. A survey and comparison of several friction force models for dynamic analysis of multibody mechanical systems. *Nonlinear Dynamics*, 86(3):1407–1443, 2016. ISSN 1573269X. doi: 10.1007/s11071-016-2999-3.

[6] D. C. Threlfall. The inclusion of Coulomb friction in mechanisms programs with particular reference to DRAM au programme DRAM. *Mechanism and Machine Theory*, 13(4):475–483, 1978. ISSN 0094114X. doi: 10.1016/0094-114X(78)90020-4.

[7] Josué Aranda-Ruiz and José Fernández-Sáez. On the use of variable-separation method for the analysis of vibration problems with time-dependent boundary conditions. *Proceedings of the Institution of Mechanical Engineers, Part C: Journal of Mechanical Engineering Science*, 226(12):2912–2924, 2012. ISSN 09544062. doi: 10.1177/0954406212442289.

[8] Hsu Chieh Yeh. Solving boundary value problems in composite media by separation of variables and transient temperature of a reactor vessel. *Nuclear Engineering and Design*, 36(2):139–157, 1976. ISSN 00295493. doi: 10.1016/0029-5493(76)90001-7.